doi:10.1093/brain/awp334 Brain 2010: 133; 847–857 | 847

BRAIN
A JOURNAL OF NEUROLOGY

Brain tissue sodium concentration in multiple sclerosis: a sodium imaging study at 3 tesla

M. Inglese,[1,2] G. Madelin,[1] N. Oesingmann,[3] J. S. Babb,[1] W. Wu,[1] B. Stoeckel,[3] J. Herbert[2] and G. Johnson[1]

1 Department of Radiology, New York University School of Medicine, 650 First Avenue, New York, NY 10016, USA
2 Department of Neurology, New York University School of Medicine, 650 First Avenue, New York, NY 10016, USA
3 Siemens Medical Solutions Inc., NY, USA

Correspondence to: Matilde Inglese,
Department of Radiology,
New York University School of Medicine,
660 1st Avenue, 4th floor,
New York,
NY 10016,
USA
E-mail: matilde.inglese@med.nyu.edu

Neuro-axonal degeneration occurs progressively from the onset of multiple sclerosis and is thought to be a significant cause of increasing clinical disability. Several histopathological studies of multiple sclerosis and experimental autoimmune encephalomyelitis have shown that the accumulation of sodium in axons can promote reverse action of the sodium/calcium exchanger that, in turn, leads to a lethal overload in intra-axonal calcium. We hypothesized that sodium magnetic resonance imaging would provide an indicator of cellular and metabolic integrity and ion homeostasis in patients with multiple sclerosis. Using a three-dimensional radial gradient-echo sequence with short echo time, we performed sodium magnetic resonance imaging at 3 T in 17 patients with relapsing–remitting multiple sclerosis and in 13 normal subjects. The absolute total tissue sodium concentration was measured in lesions and in several areas of normal-appearing white and grey matter in patients, and corresponding areas of white and grey matter in controls. A mixed model analysis of covariance was performed to compare regional tissue sodium concentration levels in patients and controls. Spearman correlations were used to determine the association of regional tissue sodium concentration levels in T_2- and T_1-weighted lesions with measures of normalized whole brain and grey and white matter volumes, and with expanded disability status scale scores. In patients, tissue sodium concentration levels were found to be elevated in acute and chronic lesions compared to areas of normal-appearing white matter ($P < 0.0001$). The tissue sodium concentration levels in areas of normal-appearing white matter were significantly higher than those in corresponding white matter regions in healthy controls ($P < 0.0001$). The tissue sodium concentration value averaged over lesions and over regions of normal-appearing white and grey matter was positively associated with T_2-weighted ($P \leqslant 0.001$ for all) and T_1-weighted ($P \leqslant 0.006$ for all) lesion volumes. In patients, only the tissue sodium concentration value averaged over regions of normal-appearing grey matter was negatively associated with the normalized grey matter volume ($P = 0.0009$). Finally, the expanded disability status scale score showed a mild, positive association with the mean tissue sodium concentration value in chronic lesions ($P = 0.002$), in regions of normal-appearing white matter ($P = 0.004$) and normal-appearing grey matter ($P = 0.002$). This study shows the feasibility of using *in vivo* sodium magnetic resonance imaging at 3 T in patients with multiple sclerosis. Our findings suggest that the abnormal values of the tissue sodium concentration in patients with relapsing–remitting multiple sclerosis might reflect changes in cellular composition of the lesions and/or changes in cellular and metabolic integrity. Sodium magnetic resonance imaging has the potential to provide insight into the pathophysiological mechanisms of tissue injury when correlation with histopathology becomes available.

Received August 17, 2009. Revised December 1, 2009. Accepted December 3, 2009. Advance Access publication January 27, 2010

Keywords: sodium imaging; multiple sclerosis; tissue sodium concentration; brain atrophy; clinical disability

Abbreviations: EDSS = expanded disability status scale; Gd = gadolinium; ^{23}Na = sodium-23; TE = echo time; TR = repetition time; TSC = tissue sodium concentration

Introduction

Neuro-axonal injury and loss are increasingly recognized as important features of multiple sclerosis, but the cellular and molecular mechanisms contributing to neurodegeneration are poorly understood (Bjartmar and Trapp, 2001). Experimental studies have revealed several mechanisms of delayed neuroaxonal loss that include demyelination, altered glial biology, aberrant glutamate homeostasis, production of nitric oxide, ion-channel alteration (Kalman *et al.*, 2007) and impairment of mitochondrial DNA and enzyme complexes (Dutta *et al.*, 2006).

Recent studies have suggested that intra-axonal sodium accumulation contributes to axonal degeneration by reversing the action of the sodium/calcium exchanger and thus inducing a lethal rise in intra-axonal calcium (Waxman, 1977, 2006; Waxman *et al.*, 1992). The functional relevance of the increased sodium influx into neurons has been demonstrated by different studies testing channel blockers such as carbamazepine, phenytoin and lamotrigine in experimental autoimmune encephalomyelitis. All these studies reported protection for axons, maintenance of axonal conduction and significant reduction in axonal degeneration in response to treatment of both monophasic and chronic-relapsing experimental autoimmune encephalomyelitis (Lo *et al.*, 2002; Bechtold *et al.*, 2004, 2006; Black *et al.*, 2007). A trial assessing neuroprotection with lamotrigine in patients with secondary-progressive multiple sclerosis has just been completed but failed to meet the primary end-point and additional trials with other sodium channel blockers are ongoing or imminent (Kapoor, 2006).

In most biological tissues, sodium is distributed in two compartments: extracellular (~140 mmol/l) and intracellular (~15 mmol/l). The observed average sodium concentration is composed of the weighted average of extra- and intracellular sodium content in the tissue, around 20 and 80%, respectively (Maudsley and Hilal, 1984). Furthermore, the ability of the cell to maintain a sodium gradient across the cell membrane, or sodium ion homeostasis, can be used as an operational definition of tissue viability.

Sodium-23 (^{23}Na) yields the second strongest nuclear magnetic resonance signal among biologically relevant nuclear magnetic resonance-active nuclei. However, there remain significant difficulties in forming magnetic resonance images of sodium. The average concentration of sodium ions in the brain is 1/2000 that of protons and the sensitivity of the ^{23}Na nucleus is ~0.092 relative to water protons (Maudsley and Hilal, 1984). In living tissues, sodium has a bi-exponential T_2 relaxation time: a short component of ~0.5–5.0 ms and a long component of 15–30 ms, with the short T_2 fraction representing 60% of the whole sodium signal. These factors all lead to intrinsically low signal-to-noise ratios.

^{23}Na MRI of the human brain was first performed >20 years ago (Hilal *et al.*, 1985), but poor signal-to-noise ratio led to relatively long imaging times and/or poor spatial resolution compared to proton (^{1}H) MRI. In addition, rapid T_2 decay makes the use of the conventional spin warp spatial encoding with echo times (TEs) of several milliseconds impractical. These limitations, combined with the sparse availability of MRI scanners with broadband capability required for ^{23}Na MRI, restricted its use to only few research sites. Interest in ^{23}Na MRI has been rekindled with the development of ultra-short TE sequences (Boada *et al.*, 1997) and the availability of ultra-high field magnets (Thulborn *et al.*, 1999) that permit better spatial resolution with shorter imaging times and better quantitative measurements of the tissue sodium concentration (TSC).

The aims of the present study were (i) to assess the presence, if any, and extent of brain regional total TSC abnormalities in patients with multiple sclerosis compared with healthy controls using ^{23}Na MRI at 3 T; (ii) to investigate the association between regional TSC levels and measures of lesion and brain volumes; and (iii) to determine possible associations between the distribution of tissue TSC changes and clinical disability from patients with multiple sclerosis.

Methods

Subjects

Seventeen patients (10 female, 7 male) diagnosed with multiple sclerosis according to the McDonald criteria (McDonald *et al.,* 2001) and presenting a relapsing–remitting (Lublin and Reingold, 1996) course were prospectively enrolled in the present study. The exclusion criteria were (i) a current or past medical or psychiatric disorder other than multiple sclerosis; (ii) current or past substance abuse and/or (iii) relapse or glucocorticosteroid use in the previous 6 weeks. Disability was assessed by a single, experienced neurologist who was blind to the MRI findings, using the expanded disability status scale (EDSS) score within 1 week of MRI. The patients had a mean age of 38.2 (range 18–53) years, a mean disease duration of 5.8 (range 2–10) years and a median EDSS score of 2.0 (range 1.0–5.0). All patients were under immunomodulatory treatment with either interferon beta-1a (Avonex, Biogen, Cambridge, MA), interferon beta-1a (Rebif, Serono, Rockland, MA) or glatiramer acetate (Copaxone, Teva, Petah Tiqvah, Israel). Thirteen age- and gender-matched healthy volunteers (10 female, 3 male) were enrolled as the control group. The mean age was 36.7 years (range 26–60). Approval for this study was obtained from the Institutional Board of Research Associates of New York University Medical Centre, and informed consent was obtained from all subjects before study initiation.

MRI acquisition

MRI was performed using a 3 T system with multi-nuclear option (MAGNETOM Trio, A Tim System, Siemens Medical Solutions, Erlangen, Germany) with a dual-tuned ^{1}H/^{23}Na transmit–receive

head volume coil (Stark Contrast, Erlangen, Germany). The following sequences were collected in all subjects during a single MRI session: (i) 3D radial gradient echo [repetition time (TR) = 120 ms; TE = 0.05 ms; 1440 radial views; flip angle = 90°; 5 averages; bandwidth = 130 Hz/pixel; field of view = 240 × 240 mm^2; matrix size = 60 × 60; nominal resolution = 4 × 4 × 4 mm^3; acquisition time = 16 min] (Madelin *et al.,* 2008). Two calibration tubes with different concentrations of sodium (100 and 50 mM) in 4% agar gel were placed in the field of view as references and allowed quantification of the sodium concentration; (ii) dual-echo turbo spin-echo (TR = 4.610 ms; TE = 10/94 ms; 36 contiguous, 4 mm thick, axial slices); (iii) 3D T_1-weighted turbo-flash magnetization-prepared rapid-acquisition gradient echo (TR = 2400 ms; TE = 2.71 ms; inversion time = 900 ms; flip angle = 12°), all slice-encoding locations acquired in a single slab, covering the whole brain, with an effective thickness of 1 mm; and (iv) post-gadolinium (Gd) T_1-weighted spin-echo (TR = 258 ms; TE = 3.16 ms; 36 contiguous, 4 mm thick axial slices).

Image processing and evaluation

All data processing was performed off-line on a PC workstation. TSC maps were calculated from the 3D radial images on a pixel-by-pixel basis as described previously (Christensen *et al.,* 1996; Nielles-Vallespin *et al.,* 2007) using Image J1.36b (http://rsb.info.nih.gov/ij/download.html). Briefly, the concentration of the calibration solutions (C_1, C_2) covered the range expected in the tissue. The signal intensities for the calibration solutions (I_1, I_2) obtained from the ^{23}Na images were then used to create a two-point linear calibration curve by solving the equation pair:

$$C_1 = aI_1 + b, \tag{1}$$

$$C_2 = aI_2 + b \tag{2}$$

for the slope a and the intercept b i.e.

$$a = \frac{C_1 - C_2}{I_1 - I_2} \tag{3}$$

$$b = \frac{C_2 I_1 - C_1 I_2}{I_1 - I_2}. \tag{4}$$

In addition, the measured intensities were divided by a correction scale $f = 0.98$ to take into account the T_1 relaxation of the calibration tubes ($T_1 \sim 30$ ms; TR = 120 ms). Using the given parameters, this factor was calculated by the following.

$$f = 1 - \exp\left(\frac{-TR}{T_1}\right) \tag{5}$$

These factors are then on a voxel-by-voxel basis over the entire ^{23}Na image to produce a TSC map:

$$\mathrm{TSC} = aI + b, \tag{6}$$

where I is the signal intensity from the brain ^{23}Na image.

Using standard propagation techniques, the error for the measured TSC can be estimated as

$$\Delta\mathrm{TSC} = \sqrt{I^2\Delta a^2 + a^2\Delta I^2 + \Delta b^2}, \tag{7}$$

with

$$\Delta a = \frac{\sqrt{\Delta C_1^2 + \Delta C_2^2 + a^2\left(\Delta I_1^2 + \Delta I_2^2\right)}}{|I_1 - I_2|} \tag{8}$$

and

$$\Delta b = \frac{\sqrt{I_2^2\Delta C_1^2 + I_1^2\Delta C_2^2 + a^2\left(I_2^2\Delta I_1^2 + I_1^2\Delta I_2^2\right)}}{|I_1 - I_2|} \tag{9}$$

Once the parametric maps were derived, TSC was measured in regions of interest for lesions and in several areas of normal-appearing white and grey matter. For all patients, lesions were identified by an experienced observer blinded to the subjects' identity on the T_2-weighted images displayed on a computer screen. To minimize partial volume effects, only lesions with a diameter greater than 5 mm were entered into the subsequent analysis. Using post-contrast T_1-weighted scans, these lesions were classified as enhancing or non-enhancing, according to previously published criteria (Barkhof *et al.,* 1997). Non-enhancing lesions were classified as T_1-isointense or hypointense. T_1 hypointensity was defined as a reduced lesion signal intensity with respect to the surrounding normal-appearing white matter. First, the standard deviation of the normal-appearing white matter signal intensity was calculated. Lesions with a signal intensity of 2 SDs lower than the surrounding normal-appearing white matter were classified as hypointense; those within 2 SDs were classified as isointense. Then, the lesions were outlined using a semi-automated segmentation technique based on local threshold (Jim version 3, Xinapse Systems, UK, http://www.xinapse.com) (Bermel *et al.,* 2003). The outlined regions of interest were automatically transferred onto the co-registered TSC maps, and the mean TSC of each lesion was measured. Finally, for each patient, the averaged TSC for enhancing lesions, T_1-isointense lesions and T_1-hypointense lesions, as well as the TSC value averaged over all lesions, was calculated. In addition, five non-enhancing hypointense lesions with a diameter of 1 cm were identified in five different patients with multiple sclerosis and the TSC level measured in the lesion centre and in three locations around the edge using circle regions of interest of 1 pixel in diameter. For all subjects, TSC values were measured in regions of normal-appearing white and grey matter. Anatomical regions of interest were selected on the T_2-weighted scans, and then transferred onto the co-registered TSC maps in order to measure the corresponding regional quantities. Circle regions of interest of variable size (range 2–8 pixels), depending on the anatomical region studied, were placed bilaterally in the following areas on two consecutive slices: splenium of the corpus callosum, white matter of the frontal and occipital lobes, peri-ventricular and cerebellar white matter, and grey matter of the frontal, parietal, temporal and occipital lobes (Fig. 1). The average TSC was calculated for every region of interest. These TSC values were then averaged over slices and sides to derive one mean TSC value for each brain region. To assess measurement variation the same observer measured the TSC of the above-mentioned white matter and grey matter areas from five healthy controls on two separate occasions, 3 months apart.

Brain volume assessment

For all subjects, normalized brain volume, normalized grey and white matter volumes were measured on magnetization-prepared rapid-acquisition gradient echo images using SIENAX as described previously (De Stefano *et al.*, 2003). SIENAX automatically segments brain from non-brain matter, calculates the brain volume and applies a normalization factor to correct for skull size (Smith *et al.,* 2002).

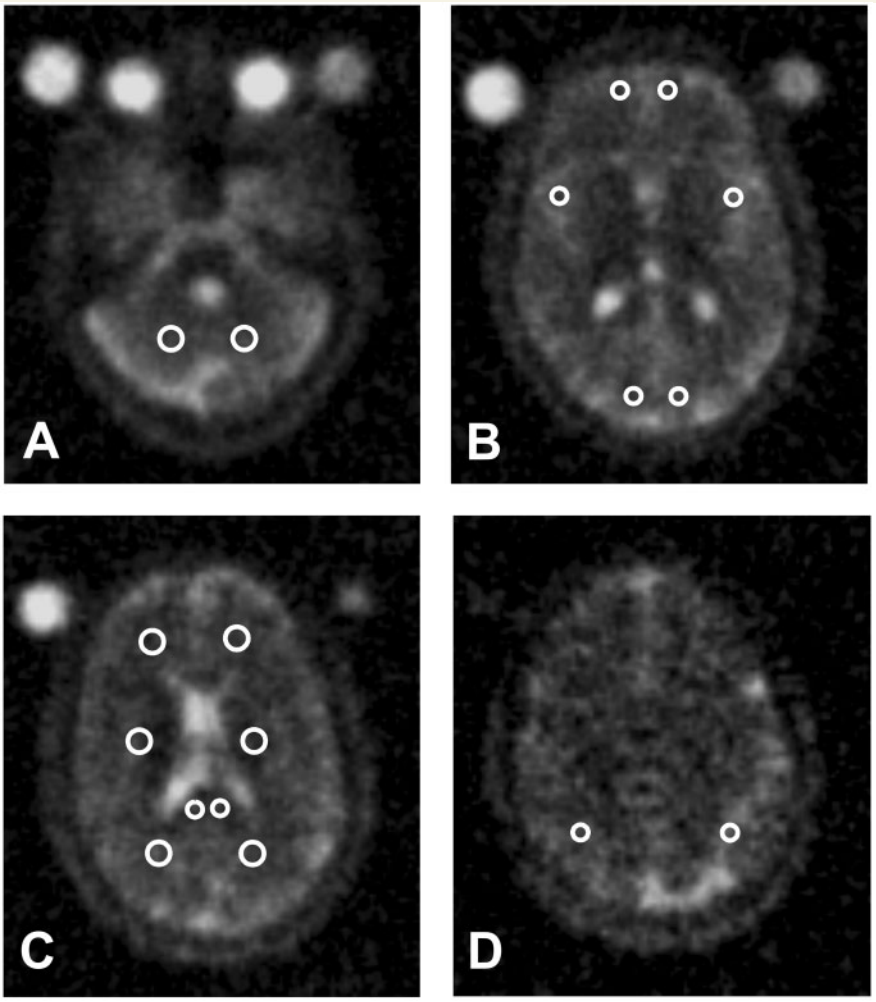

Figure 1 Location of the white matter and grey matter regions of interest on selected TSC maps in a healthy volunteer. (**A**) White matter of cerebellar lobes. (**B**) Grey matter of frontal, parietal and occipital lobes. (**C**) Periventricular white matter, splenium of the corpus callosum, white matter of the frontal and occipital lobes. (**D**) Grey matter of parietal lobes. See the text for further details.

To correct for misclassification of T_1-weighted grey matter volume in the presence of high T_1-weighted hypointense lesion volume (Nakamura and Fisher, 2009), each T_1-weighted hypointense lesion of each subject was filled with the mean intensity value of the normal appearing white matter present in the same slice of the lesion.

Lesion volume assessment

For all patients, T_2-hyperintense and T_1-hypointense lesion volume measurements were performed by a single experienced observer, blinded to the subject's identity, using a semi-automated segmentation technique based on user-supervised local thresholding (Jim version 3; Xinapse Systems, Northants, England) (http://www.xinapse.com). For the T_2-weighted lesion volume classification, lesion borders were determined on proton density-weighted images using the T_2-weighted images as reference. T_1-hypointense lesions were defined as those lesions with signal intensity between that of the grey matter and the CSF on T_1-weighted scans (van Waesberghe *et al.*, 1998). In both T_2- and T_1-weighted images, the value of total brain lesion volume was calculated by multiplying lesion area by slice thickness.

Statistical analysis

Statistical Analysis System version 9.0 (SAS Institute, Cary, NC) was used for all statistical computations. Mixed model analysis of covariance was used to compare patients and controls in terms of regional TSC levels. The TSC assessments constituted the dependent variable with a separate analysis conducted for each brain region. Subject group (MS, controls) and gender were included in the model as fixed classification factors and subject age was included as a numeric covariate. Group differences were tested using type 3 *P*-values in order to assess differences adjusted for age and gender. Mixed model ANOVA was used to compare brain regions and lesion types in terms of the TSC value observed for patients. For this analysis, the TSC levels from all brain regions of patients represented the dependent variable, and the model included the indicator variable identifying the brain region or lesion type associated with each observation as a fixed classification factor. Age and gender were excluded from the model since brain regions were compared within subjects. In all mixed model analyses, the covariance structure was modelled by assuming observations to be correlated only when acquired from the same subject and by allowing the error variance to differ across subject groups, lesion

types and brain regions. Unequal variance *t*-tests were used to assess gender differences in terms of the mean TSC value. Analysis of covariance was used to assess the possibility of a Gender × Group interaction. TSCs in the white matter and grey matter were modelled as dependent variables in separate analyses and each dependent variable was modelled as a function of Gender, Group and the Gender × Group interaction. The analysis allowed the error variance to differ across groups. Spearman's rank correlation coefficients were used to characterize the association of TSC measures with disease duration, brain and volume measures and with the EDSS score. Restricted maximum likelihood estimation of variance components in a random effects model was used to assess intra-observer variation in the replicate assessment of TSC made by one observer on two separate occasions for each of the five controls. Results are summarized as the intra-observer coefficient of variation and intra-class correlation coefficient. Results were declared statistically significant when associated with a *P*-value <0.05. While *P*-values are reported without multiple comparison correction, explicit mention is made regarding results that would remain significant after Tukey's honestly significant difference or Bonferroni adjustment for multiple comparisons.

Results

TSC levels in white and grey matter tissue in healthy controls

The mean ± SD of TSC values in white and grey matter regions from healthy controls are reported in Table 1. Among white matter regions, TSC values in the cerebellum and in the splenium of the corpus callosum were significantly higher than in periventricular regions ($P = 0.0006$ and $P = 0.0004$). There were no significant differences in TSC levels among grey matter regions ($P \geqslant 0.9$). TSC was significantly higher in the grey matter than in the white matter regions ($P < 0.0001$) (Fig. 2). On two separate occasions (3 months apart), the same observer measured the TSC

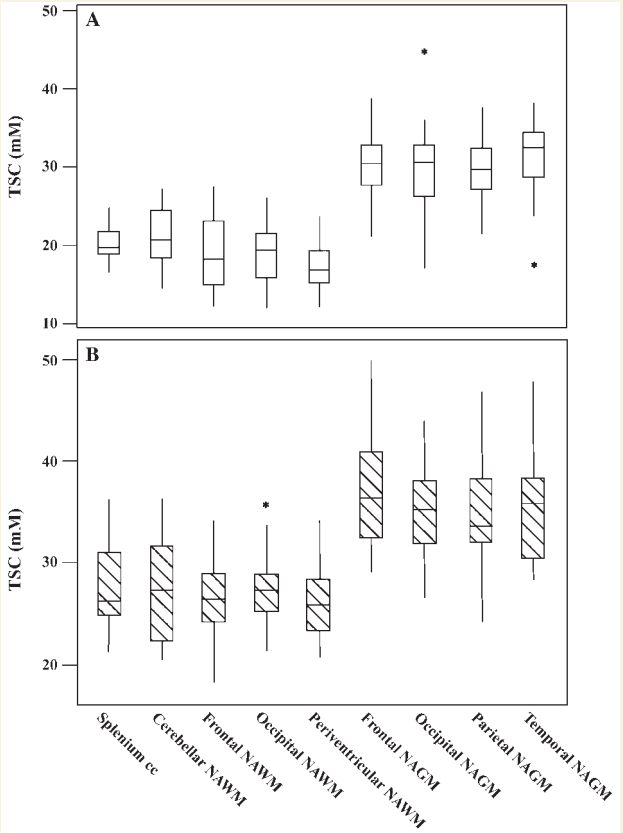

Figure 2 Box plots displaying the 25–75% values (boxes) ± 95% values (whiskers), median values (horizontal lines within boxes) and outliers (asterisk) of the mean TSC value distribution in regions of white matter and grey matter among healthy controls (**A**, empty box) and in corresponding normal-appearing white matter (NAWM) and normal-appearing grey matter (NAGM) regions among patients with relapsing–remitting multiple sclerosis (**B**, hatched box). cc = corpus callosum.

Table 1 The mean brain regional tissue sodium concentration level in healthy controls and patients with relapsing–remitting multiple sclerosis

Brain region	Controls	Multiple sclerosis patients	*P*-value
Frontal NAWM	19.07 ± 4.53	25.49 ± 5.44	0.003
Occipital NAWM	19.08 ± 3.68	25.81 ± 5.62	0.001
Splenium corpus callosum	20.26 ± 2.35	28.14 ± 5.23	<0.0001
Periventricular NAWM	17.22 ± 2.70	24.02 ± 5.45	0.0003
Whole NAWM	19.38 ± 1.65	26.94 ± 3.12	<0.0001
Cerebellum NAWM	21.28 ± 3.62	28.61 ± 5.69	0.0005
Frontal NAGM	30.22 ± 4.77	37.28 ± 6.73	0.005
Occipital NAGM	30.34 ± 6.28	35.93 ± 4.82	0.02
Parietal NAGM	30.00 ± 4.14	34.64 ± 5.64	0.02
Temporal NAGM	31.58 ± 4.30	37.78 ± 4.75	0.002
Whole NAGM	30.54 ± 3.17	35.59 ± 4.16	<0.0001
Hypointense lesions (67)	–	39.19 ± 8.09	–
Isointense lesions (25)	–	30.11 ± 7.02	–
Gd-enhancing lesions (4)	–	40.93 ± 17.15	–
All lesions	–	35.34 ± 9.45	–

TSC values in (mM) ± standard deviation. Each *P*-value is from the mixed model analysis of covariance to compare relapsing–remitting multiple sclerosis patients to healthy controls in terms of TSC levels adjusted for age and gender. NAWM = normal-appearing white matter; NAGM = normal-appearing grey matter.

of the above-mentioned white matter and grey matter areas from five healthy controls. The repeated studies on five controls showed a coefficient of variation for TSC smaller than 5% and an intra-class correlation coefficient >0.9 for all the white and the grey matter regions studied.

TSC levels in lesions and normal-appearing white matter and grey matter tissue in patients with relapsing–remitting multiple sclerosis

The mean ± SD of TSC values from lesions, normal-appearing white matter and grey matter regions of patients are reported in Table 1 and the regional distribution of TSC values in comparison to healthy controls is described in Fig. 2. TSC was measured only in lesions with a diameter >5 mm to minimize partial volume effect (Fig. 3). Using post-contrast T_1-weighted scans, these lesions were classified as enhancing and non-enhancing; the latter were then classified as T_1-isointense or hypointense. TSC levels were measured in 4 Gd-enhancing, 25 isointense and 67 hypointense lesions. An averaged TSC value over all lesions was also measured. While the TSC level in Gd-enhancing and hypointense lesions were statistically indistinguishable, only the latter had significantly higher TSC when compared to that of isointense lesions ($P < 0.0001$). TSC level in hypointense lesions was significantly higher than that in regions of normal-appearing white matter ($P < 0.0001$) but not different from that in regions of normal-appearing grey matter ($P = 0.1$) (Fig. 4). The TSC value of isointense lesions was significantly higher than that of frontal ($P = 0.009$) and periventricular normal-appearing white matter ($P = 0.007$). The TSC value of isointense lesions was significantly higher than that of TSC averaged over regions of normal-appearing white matter ($P = 0.03$) but the significance was not retained after Tukey's adjustment for multiple comparisons ($P \geqslant 0.1$). In contrast, the TSC level of isointense lesions was significantly lower than that of normal-appearing grey matter regions ($P < 0.0001$) (Fig. 4). Finally, the TSC level averaged over the centre of the five non-enhancing hypointense lesions

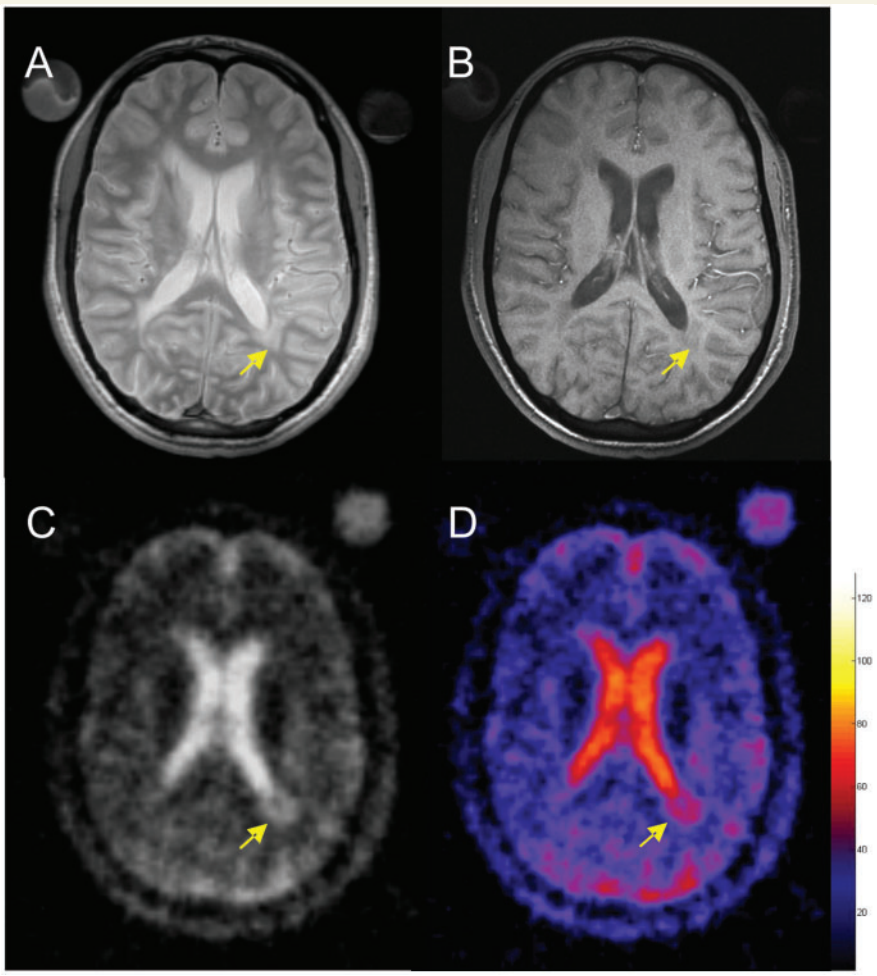

Figure 3 Selected brain axial proton density (**A**), T_1-weighted (**B**), ^{23}Na images (**C**) and corresponding TSC map (**D**) from a 29-year-old patient with multiple sclerosis. The colour bar indicates the TSC values (mM). Note the higher TSC value in the periventricular lesion that appears hypointense (arrow) on the T_1-weighted image (**B**).

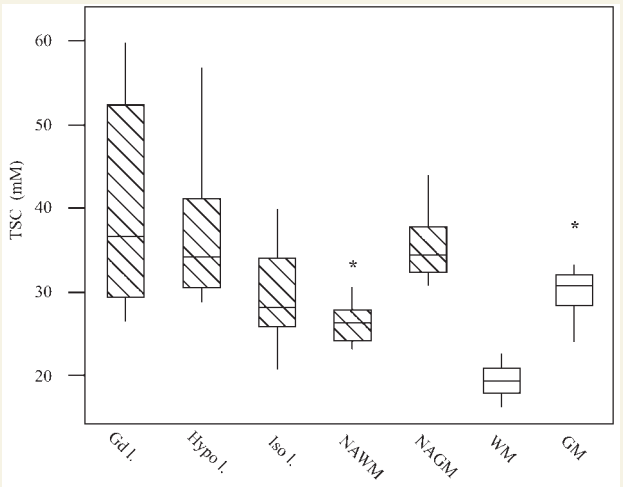

Figure 4 Box plots displaying the 25–75% values (boxes) ± 95% values (whiskers), median values (horizontal lines within boxes) and outliers (asterisk) of the mean TSC value distribution in Gd-enhancing (Gd 1; 4), hypointense (Hypo 1; 67), isointense (Iso 1; 25) lesions and in normal-appearing white matter (NAWM) and normal-appearing grey matter (NAGM) regions among patients with multiple sclerosis (hatched box) and in the corresponding white matter (WM) and grey matter (GM) regions among healthy controls (empty box). Note that the TSC level of Gd-enhancing and hypointense lesions was statistically indistinguishable. The TSC level in hypointense lesions was significantly higher than that in isointense lesions ($P < 0.0001$) and that in regions of normal-appearing white matter ($P < 0.0001$) but not different from that of normal-appearing grey matter regions ($P = 0.1$). In contrast, the TSC level of isointense lesions was significantly lower than that of normal-appearing grey matter regions ($P < 0.0001$) but not statistically distinguishable from that of TSC averaged over normal-appearing white matter regions after Tukey's adjustment for multiple comparisons ($P = 0.1$).

with a diameter of 1 cm was 51.4 ± 6.0 mM, whereas the TSC level averaged over the lesion edge was 38.8 ± 4.8 mM. Although the TSC values in the cerebellum and in the splenium of the corpus callosum were significantly higher than that in periventricular normal-appearing white matter ($P = 0.007$ and $P = 0.02$), the significance was not retained after Tukey's adjustment for multiple comparisons ($P \geqslant 0.1$). There were no significant differences in terms of TSC levels among normal-appearing grey matter regions ($P \geqslant 0.3$), whereas the TSC value in the regions of normal-appearing grey matter was significantly higher than that in regions of normal-appearing white matter ($P < 0.0001$).

Comparison between normal-appearing white matter, normal-appearing grey matter and corresponding TSC levels

No significant associations were found between age or gender and the mean TSC levels in either patients ($P = 0.8$) or controls ($P = 0.9$). Likewise, no significant Gender × Group interaction was found in terms of either white matter TSC ($P = 0.2$) or grey matter TSC ($P = 0.4$). In healthy controls, the mean ± SD of TSCs in the white matter and grey matter were 19.37 ± 1.79 and 30.30 ± 1.37 mM, respectively, in the males, and 19.38 ± 1.69 and 30.64 ± 3.79 mM, respectively, in the females. In patients, the mean ± SD of TSC in the white matter and grey matter were 28.15 ± 4.19 and 36.65 ± 5.62 mM, respectively, in the males and 26.09 ± 1.90 and 34.84 ± 2.87 mM, respectively, in the females. After adjusting for age and gender, significant differences in TSC levels were found between patients with relapsing–remitting multiple sclerosis and the healthy controls in regions of both white matter (range <0.0001–0.0003) and grey matter (range 0.002–0.03). All *P*-values except three (normal-appearing grey matter of parietal, temporal and occipital lobes) remained significant after a Bonferroni correction. Results of group comparisons with respect to average regional TSC are reported in Table 1.

Correlations among brain TSC values, lesion and brain volumes

In patients, the T_2-weighted lesion volume was 6.12 ± 7.90 ml and the T_1-weighted lesion volume was 2.66 ± 5.40 ml. The TSC value averaged over lesions was positively associated with the T_2-weighted ($r = 0.44$, $P = 0.0001$) and the T_1-weighted ($r = 0.44$, $P = 0.0001$) lesion volume. In particular, the TSC averaged over hypointense lesions was positively associated with the T_1-weighted lesion volume ($r = 0.47$, $P = 0.0003$). Likewise, the TSC value averaged over regions of normal-appearing white matter and normal-appearing grey matter was positively associated with the T_2-weighted ($r = 0.41$, $P = 0.0001$ and $r = 0.37$, $P = 0.001$, respectively) and the T_1-weighted ($r = 0.31$, $P = 0.0002$ and $r = 0.28$, $P = 0.006$, respectively) lesion volume.

The patients had a significantly lower normalized brain volume (1533.1 ± 116.9 ml; $P = 0.009$) and grey matter volume (832.6 ± 84.4 ml; $P = 0.007$), but only a trend for lower white matter volume (694.0 ± 52.4 ml; $P = 0.06$) compared with healthy controls (normalized brain volume: 1634.8 ± 59.0 ml; grey matter volume: 901.8 ± 58.4 ml; white matter volume: 732.9 ± 61.8 ml).

In patients, the TSC value averaged over regions of normal-appearing grey matter was negatively associated with the grey matter volume ($r = -0.23$, $P = 0.0009$) but not with the normalized brain volume ($P = 0.3$) whereas TSC averaged over regions of normal-appearing white matter was associated neither with the white matter volume nor with the normalized brain volume ($P = 0.1$ for both). In control subjects, the TSC values averaged over regions of white matter and grey matter were inversely associated with the normalized brain volume ($r = -0.20$, $P = 0.001$; $r = -0.43$, $P = 0.0001$, respectively) but they did not show any significant association with the corresponding white matter or grey matter volume ($P = 0.1$ for both).

Correlations among TSC values, disease duration and EDSS

Neither the TSC level in lesions ($P = 0.6$) nor that in normal-appearing white matter ($P = 0.5$) and grey matter ($P = 0.1$) was significantly associated with disease duration. With respect to the EDSS score, a mild, positive correlation was found with the mean TSC value in the T_1-weighted hypointense lesions ($r = 0.22$, $P = 0.002$), the mean TSC value in the normal-appearing white matter ($r = 0.20$, $P = 0.004$) and the mean TSC value in the normal-appearing grey matter ($r = 0.20$, $P = 0.002$).

Discussion

One of the most challenging aspects of multiple sclerosis is to understand the nature and mechanism of tissue injury. Conventional and advanced MRI techniques have had an enormous impact in enabling early diagnosis, evaluation of treatment regimens and enhancing the understanding of multiple sclerosis pathophysiology (Miller *et al.,* 2004; Bakshi *et al.,* 2008). However, MRI methods for exact identification and quantification of mechanisms of tissue injury *in vivo* are lacking and the study of degeneration remains limited by the paucity of pathological data from the early stage of the disease. To our knowledge this is the first application of ^{23}Na MRI in a group of patients with multiple sclerosis. ^{23}Na MRI can provide an indicator of cellular and metabolic integrity and ion homeostasis *in vivo* and has already been employed to study neurological disorders such as ischaemic stroke, brain tumours and Alzheimer's disease (Thulborn *et al.,* 1999; Ouwerkerk *et al.,* 2003; Mellon *et al.,* 2009).

In the present study, the brain TSC distribution of healthy controls was quite homogeneous among regions of white matter (except for lower values in the periventricular area) and among regions of grey matter. The TSC of grey matter regions, however, was significantly higher than that of white matter regions, in line with the findings of previous studies in healthy subjects (Perman *et al.,* 1986; Thulborn *et al.,* 2005). The brain TSC distribution of patients with multiple sclerosis revealed the highest levels of TSC in Gd-enhancing and T_1-hypointense lesions, whereas the TSC of T_1-isointense lesions was lower than that of T_1-hypointense lesions but higher than that of regions of normal-appearing white matter. An increased TSC, albeit to a lesser extent, was also found in regions of normal-appearing white matter when compared with corresponding regions of white matter from healthy controls.

Since TSC represents the weighted average of extracellular and intracellular sodium in the examined tissue, the increased value observed in patients with multiple sclerosis could reflect both an increase of extracellular space due to vasogenic oedema and/or cell loss and demyelination as well as an increase of the intracellular sodium due to inflammatory-related over-expression of cellular membrane sodium channels and/or hypercellularity. Since persistent T_1-hypointense lesions are characterized by severe tissue destruction (Bruck *et al.,* 1997; van Walderveen *et al.,* 1998; van Waesberghe *et al.,* 1999), the increase of extracellular sodium is likely to play a major role in chronic lesions, where most of the lost tissue has been replaced by fluid. This is partially supported by the positive association found in our study between TSC averaged over T_1-hypointense lesions and the T_1-weighted lesion volume. The association, however, was only moderate, suggesting that mechanisms other than an increase of the extracellular fluid subsequent to myelin and axonal loss accounts, at least partially, for the observed increase of TSC. It is well known that T_1-hypointensities are quite heterogeneous (Barkhof *et al.,* 2003) and due to the cross-sectional design of our study we were not able to distinguish permanent from temporary T_1-hypointense lesions. Furthermore, although the small number of examined lesions precluded a statistical analysis, the TSC levels measured in the centre of chronic lesions were higher than those measured at lesion edge, which in turn were higher than the TSC levels measured in regions of normal-appearing white matter. This suggests the presence of TSC gradient from the centre to the periphery of lesions that might reflect underlying increase of the extracellular space in the necrotic centre and the presence of higher cellularity with few surviving axons, astrocytic processes and sparse remyelination at the edge (Lassmann, 2008).

An increase in extracellular sodium is also likely to play a major role in Gd-enhancing lesions, at least until the resolution of oedema (Turski *et al.,* 1986) and inflammation. We speculate that additional contribution to the increased TSC found in acute lesions might be provided by the increase in cellular volume fraction due to the presence of inflammatory cells. Unfortunately, the small number of Gd-enhancing lesions found in our group of patients prevented an evaluation of any associations with T_2-weighted lesions and brain volumes. Serial studies on a larger number of new Gd-enhancing lesions with ^{23}Na MRI are needed in order to clarify the value of such observations, especially after the resolution of inflammation.

Particular attention in terms of providing a pathophysiological interpretation of our findings should be paid to recent studies demonstrating sustained intra-axonal sodium accumulation through voltage-gated sodium channels. As a consequence of the intracellular Na overload, the action of sodium/calcium exchanger is reversed, inducing a lethal rise of calcium and calcium-mediated processes after the axons are exposed to insults such as anoxia and demyelination (Waxman, 2006). It has been demonstrated that demyelinated axons can develop a higher-than-normal density of sodium channels along the axon membrane (Waxman, 1977; Foster *et al.,* 1980; England *et al.,* 1991; Moll *et al.,* 1991). Although the expression of some sodium channel isoforms may have an adaptive role in restoring conduction interrupted by the loss of myelin, other isoforms such as $Na_v1.6$ (Craner *et al.,* 2004*b*) may have a maladaptive role contributing to axonal degeneration. Specifically, since $Na_v1.6$ channels produce a larger persistent current than other sodium channels, co-expression of $Na_v1.6$ channels and the sodium/calcium exchanger (Herzog *et al.,* 2003) would be expected to predispose demyelinated axons to import injurious levels of calcium. Using triple-immunofluorescent labelling, Craner and colleagues have provided evidence that the coexpression of sodium channel $Na_v1.6$ and the sodium/calcium exchanger are associated with axonal injury within acute lesions in experimental autoimmune encephalomyelitis and post-mortem multiple sclerosis tissue (Craner *et al.,* 2004*a*, *b*). The link between sodium channels and

axonal degeneration in neuroinflammation is supported by the demonstration that the sodium channel blockers phenytoin, flecainide and lamotrigine have protective effects in experimental autoimmune encephalomyelitis by reducing axonal degeneration, maintaining the ability of axons to conduct impulses and improving clinical outcome (Lo *et al.,* 2002; Bechtold *et al.,* 2004, 2006). Furthermore, it has been shown that nitric oxide produced in inflammatory lesions can reduce cellular ATP production by interfering with mitochondrial electron transport (Smith and Lassmann, 2002). ATP depletion, in turn, induces a failure of the sodium/potassium-ATPase with an increase of the intracellular sodium concentration and changes in the resting potential of the neuronal membrane that trigger axonal degeneration (Smith *et al.,* 2001) that can be prevented by pharmacological blockade of sodium channels (Kapoor *et al.,* 2003).

Altogether, these observations might explain increased TSC in the absence of increases in extracellular water and sodium. Although any attempt to interpret the underlying substrate of TSC changes is speculative and could only be confirmed by a post-mortem examination, we believe that unlike in T_1-hypointense lesions, increases in intracellular sodium might explain, at least partially, our findings in Gd-enhancing T_1-isointense lesions and regions of normal-appearing white matter. Several studies have reported that multiple sclerosis lesions are frequently initially hypointense, with around a third reverting back to isointensity at follow-up (Dousset *et al.,* 1998; Rovira *et al.,* 1999; Bitsch *et al.,* 2001). Other studies have shown that isointense lesions have significantly higher magnetization transfer ratio values than severely hypointense lesions (Barkhof *et al.,* 2003). A more recent pathologic–radiological study performed with patients who underwent brain biopsy for diagnostic reasons found that lesions in the stage of early remyelination showed a tendency to develop from hypointense initially to more isointense over time (Bitsch *et al.,* 2001). Although the speculation that the increase of TSC in isointense lesions might be related to reparative mechanisms is intriguing, only a serial MRI study (Barkhof *et al.,* 2003) will help clarify the pathophysiological significance of lesional changes of TSC. Finally, in a recent report, Craner *et al.* (2005) found that sodium channels are also present in macrophages and microglial cells, and that the expression of Na_v 1.6 channels is increased in activated microglia and macrophages in post-mortem multiple sclerosis tissue and experimental autoimmune encephalomyelitis (Craner *et al.,* 2005). Moreover, it is now well-established that astrocytes can express sodium channels, in some cases in densities high enough to support action potential generation if resting inactivation is removed (Sontheimer and Waxman, 1992), and there is evidence suggesting that sodium channel activity may be essential for the viability of astrocytes (Sontheimer *et al.,* 1994). Thus, the increase of TSC we found in multiple sclerosis lesions could be of glial and axonal origin.

Another interesting finding of our study is the observed increase of TSC in regions of normal-appearing white matter. It is well known that normal-appearing white matter, as defined by MRI, is abnormal in the majority of cases (Allen *et al.,* 2001). The pathological basis of these abnormalities includes astrogliosis, vascular hyalination, reduced myelin density, remyelination, axonal loss, perivascular inflammation and microplaque formation (Allen and McKeown, 1979; Gay and Esiri, 1991; Bjartmar *et al.,* 2001). The increased TSC observed in our study might be explained by increased extracellular space due to demyelination and axonal loss that are present in normal-appearing white matter. However, a relationship between increased intracellular sodium and TSC elevation cannot be excluded. In keeping with this perspective, we did not find any significant association between the TSC values averaged over normal-appearing white matter regions and the normalized white matter volume. Another interesting speculation has been provided by DeLuca *et al.* (2006) who found only a weak correlation between axonal loss and plaque load in post-mortem multiple sclerosis tissue, raising the point that demyelination might not be a prime determinant of axonal degeneration in multiple sclerosis. The sodium/calcium exchanger is in fact present at intact nodes where Nav1.6 channels are aggregated in normal white matter. Therefore, if the inadequacy of ATP supply described by Dutta and colleagues (2006) in multiple sclerosis occurs in neurons in which axons are not demyelinated, the axons may be poised to undergo calcium-mediated injury.

Disappointingly, we found only a modest correlation between the increase of TSC in lesions and normal-appearing white matter and grey matter, and the EDSS score. However, in addition to the well-known limitations of the EDSS scale (Balcer, 2001) and the narrow range of EDSS scores of our patients, it is possible that TSC reflects, at least in part, a dynamic pathological process rather than tissue damage *per se* and as such it might serve better as a predictive factor of clinical outcome. Future studies will focus on the entire range of clinical stages including patients with clinically isolated syndrome and patients with secondary and primary progressive multiple sclerosis.

This study has a number of limitations. First, due to the relatively small patient sample, our findings have to be regarded as preliminary and their interpretation has to be cautious. It is important to confirm these findings in a larger patient group, examined serially from the early stage of the disease. Second, the available ^{23}Na MRI method did not allow discrimination between extra- and intracellular tissue sodium that would have provided more physiologically relevant information. Technical implementations of triple quantum filtered ^{23}Na MRI, ongoing at our centre at high magnetic field strength, will enable separate investigations of the intra- and extracellular sodium compartments. Third, the effect of immunomodulatory treatment on brain TSC is not known. Therefore, ^{23}Na studies in patients with multiple sclerosis before and after immunomodulating therapy are needed in order to assess for a possible effect of treatment. Finally, only lesions with a diameter $\geqslant$5 mm were studied due to the relatively low resolution of ^{23}Na images. This problem will be partially overcome by the future use of high-sensitivity coil arrays, higher field strength and by the acquisition of more averages.

In summary, we report here the results of the first study assessing brain TSC distribution in patients with relapsing–remitting multiple sclerosis. Increases in TSC were observed in lesions and, to a lesser extent, in the normal-appearing white matter and grey matter of patients, in comparison to healthy controls. An inverse, weak correlation was found between the increase of TSC in grey matter and measures of grey matter volume. This is very

interesting in the light of the findings of a study of sodium imaging in patients with Alzheimer's disease (Mellon *et al.*, 2009). In this preliminary study, the increase in sodium signal intensity was found to correlate inversely with hippocampal volume but the sodium signal intensities differences could not be explained entirely by changes in hippocampal volumes. Although our findings in grey matter TSC suggest that ^{23}Na MRI can provide complementary information on tissue injury at a cellular level, the association between grey matter volume and grey matter TSC could be equally explained by the partial volume effect. By contrast, no significant association was found between the increase of TSC averaged over regions of normal-appearing white matter and measures of white matter volume, suggesting that TSC might represent an earlier marker of tissue injury.

Acknowledgements

The authors would like to thank Dr Sonia Nielles-Vallespin from Siemens Medical Solutions Erlangen, Germany, for her help in pulse sequence development.

Funding

This study was supported in part by the US National Institute of Health (grant number RO1 NS051623).

References

Allen IV, McKeown SR. A histological, histochemical and biochemical study of the macroscopically normal white matter in multiple sclerosis. J Neurol Sci 1979; 41: 81–91.

Allen IV, McQuaid S, Mirakhur M, Nevin G. Pathological abnormalities in the normal-appearing white matter in multiple sclerosis. Neurol Sci 2001; 22: 141–4.

Bakshi R, Thompson AJ, Rocca MA, Pelletier D, Dousset V, Barkhof F, et al. MRI in multiple sclerosis: current status and future prospects. Lancet Neurol 2008; 7: 615–25.

Balcer LJ. Clinical outcome measures for research in multiple sclerosis. J Neuroophthalmol 2001; 21: 296–301.

Barkhof F, Bruck W, De Groot CJ, Bergers E, Hulshof S, Geurts J, et al. Remyelinated lesions in multiple sclerosis: magnetic resonance image appearance. Arch Neurol 2003; 60: 1073–81.

Barkhof F, Filippi M, van Waesberghe JH, Molyneux P, Rovaris M, Lycklama a Nijeholt G, et al. Improving interobserver variation in reporting gadolinium-enhanced MRI lesions in multiple sclerosis. Neurology 1997; 49: 1682–8.

Bechtold DA, Kapoor R, Smith KJ. Axonal protection using flecainide in experimental autoimmune encephalomyelitis. Ann Neurol 2004; 55: 607–16.

Bechtold DA, Miller SJ, Dawson AC, Sun Y, Kapoor R, Berry D, et al. Axonal protection achieved in a model of multiple sclerosis using lamotrigine. J Neurol 2006; 253: 1542–51.

Bermel RA, Sharma J, Tjoa CW, Puli SR, Bakshi R. A semiautomated measure of whole-brain atrophy in multiple sclerosis. J Neurol Sci 2003; 208: 57–65.

Bitsch A, Kuhlmann T, Stadelmann C, Lassmann H, Lucchinetti C, Bruck W. A longitudinal MRI study of histopathologically defined hypointense multiple sclerosis lesions. Ann Neurol 2001; 49: 793–6.

Bjartmar C, Kinkel RP, Kidd G, Rudick RA, Trapp BD. Axonal loss in normal-appearing white matter in a patient with acute MS. Neurology 2001; 57: 1248–52.

Bjartmar C, Trapp BD. Axonal and neuronal degeneration in multiple sclerosis: mechanisms and functional consequences. Curr Opin Neurol 2001; 14: 271–8.

Black JA, Liu S, Carrithers M, Carrithers LM, Waxman SG. Exacerbation of experimental autoimmune encephalomyelitis after withdrawal of phenytoin and carbamazepine. Ann Neurol 2007; 62: 21–33.

Boada FE, Gillen JS, Shen GX, Chang SY, Thulborn KR. Fast three dimensional sodium imaging. Magn Reson Med 1997; 37: 706–15.

Bruck W, Bitsch A, Kolenda H, Bruck Y, Stiefel M, Lassmann H. Inflammatory central nervous system demyelination: correlation of magnetic resonance imaging findings with lesion pathology. Ann Neurol 1997; 42: 783–93.

Christensen JD, Barrere BJ, Boada FE, Vevea JM, Thulborn KR. Quantitative tissue sodium concentration mapping of normal rat brain. Magn Reson Med 1996; 36: 83–9.

Craner MJ, Damarjian TG, Liu S, Hains BC, Lo AC, Black JA, et al. Sodium channels contribute to microglia/macrophage activation and function in EAE and MS. Glia 2005; 49: 220–9.

Craner MJ, Hains BC, Lo AC, Black JA, Waxman SG. Co-localization of sodium channel Nav1.6 and the sodium-calcium exchanger at sites of axonal injury in the spinal cord in EAE. Brain 2004a; 127: 294–303.

Craner MJ, Newcombe J, Black JA, Hartle C, Cuzner ML, Waxman SG. Molecular changes in neurons in multiple sclerosis: altered axonal expression of Nav1.2 and Nav1.6 sodium channels and Na+/Ca2+ exchanger. Proc Natl Acad Sci USA 2004b; 101: 8168–73.

De Stefano N, Matthews PM, Filippi M, Agosta F, De Luca M, Bartolozzi ML, et al. Evidence of early cortical atrophy in MS: relevance to white matter changes and disability. Neurology 2003; 60: 1157–62.

DeLuca GC, Williams K, Evangelou N, Ebers GC, Esiri MM. The contribution of demyelination to axonal loss in multiple sclerosis. Brain 2006; 129: 1507–16.

Dousset V, Gayou A, Brochet B, Caille JM. Early structural changes in acute MS lesions assessed by serial magnetization transfer studies. Neurology 1998; 51: 1150–5.

Dutta R, McDonough J, Yin X, Peterson J, Chang A, Torres T, et al. Mitochondrial dysfunction as a cause of axonal degeneration in multiple sclerosis patients. Ann Neurol 2006; 59: 478–89.

England JD, Gamboni F, Levinson SR. Increased numbers of sodium channels form along demyelinated axons. Brain Res 1991; 548: 334–7.

Foster RE, Whalen CC, Waxman SG. Reorganization of the axon membrane in demyelinated peripheral nerve fibers: morphological evidence. Science 1980; 210: 661–3.

Gay D, Esiri M. Blood–brain barrier damage in acute multiple sclerosis plaques. An immunocytological study. Brain 1991; 114: 557–72.

Herzog RI, Cummins TR, Ghassemi F, Dib-Hajj SD, Waxman SG. Distinct repriming and closed-state inactivation kinetics of Nav1.6 and Nav1.7 sodium channels in mouse spinal sensory neurons. J Physiol 2003; 551: 741–50.

Hilal SK, Maudsley AA, Ra JB, Simon HE, Roschmann P, Wittekoek S, et al. In vivo NMR imaging of sodium-23 in the human head. J Comput Assist Tomogr 1985; 9: 1–7.

Kalman B, Laitinen K, Komoly S. The involvement of mitochondria in the pathogenesis of multiple sclerosis. J Neuroimmunol 2007; 188: 1–12.

Kapoor R. Neuroprotection in multiple sclerosis: therapeutic strategies and clinical trial design. Curr Opin Neurol 2006; 19: 255–9.

Kapoor R, Davies M, Blaker PA, Hall SM, Smith KJ. Blockers of sodium and calcium entry protect axons from nitric oxide-mediated degeneration. Ann Neurol 2003; 53: 174–80.

Lassmann H. The pathologic substrate of magnetic resonance alterations in multiple sclerosis. Neuroimaging Clin N Am 2008; 18: 563–76, ix.

Lo AC, Black JA, Waxman SG. Neuroprotection of axons with phenytoin in experimental allergic encephalomyelitis. Neuroreport 2002; 13: 1909–12.

Lublin FD, Reingold SC. Defining the clinical course of multiple sclerosis: results of an international survey. National Multiple Sclerosis Society (USA) Advisory Committee on Clinical Trials of New Agents in Multiple Sclerosis. Neurology 1996; 46: 907–11.

Madelin G, Oesingmann N, Nielles-Vallespin S, Herbet J, Johnson G, Inglese M. 3 T Sodium MRI of Patients with Multiple Sclerosis. Toronto, Canada: International Society for Magnetic Resonance in Medicine (ISMRM), 2008.

Maudsley AA, Hilal SK. Biological aspects of sodium-23 imaging. Br Med Bull 1984; 40: 165–6.

McDonald WI, Compston A, Edan G, Goodkin D, Hartung HP, Lublin FD, et al. Recommended diagnostic criteria for multiple sclerosis: guidelines from the International Panel on the diagnosis of multiple sclerosis. Ann Neurol 2001; 50: 121–7.

Mellon EA, Pilkinton DT, Clark CM, Elliott MA, Witschey WR, 2nd, Borthakur A, et al. Sodium MR imaging detection of mild Alzheimer disease: preliminary study. AJNR Am J Neuroradiol 2009; 30: 978–84.

Miller DH, Filippi M, Fazekas F, Frederiksen JL, Matthews PM, Montalban X, et al. Role of magnetic resonance imaging within diagnostic criteria for multiple sclerosis. Ann Neurol 2004; 56: 273–8.

Moll C, Mourre C, Lazdunski M, Ulrich J. Increase of sodium channels in demyelinated lesions of multiple sclerosis. Brain Res 1991; 556: 311–6.

Nakamura K, Fisher E. Segmentation of brain magnetic resonance images for measurement of gray matter atrophy in multiple sclerosis patients. Neuroimage 2009; 44: 769–76.

Nielles-Vallespin S, Weber MA, Bock M, Bongers A, Speier P, Combs SE, et al. 3D radial projection technique with ultrashort echo times for sodium MRI: clinical applications in human brain and skeletal muscle. Magn Reson Med 2007; 57: 74–81.

Ouwerkerk R, Bleich KB, Gillen JS, Pomper MG, Bottomley PA. Tissue sodium concentration in human brain tumors as measured with 23Na MR imaging. Radiology 2003; 227: 529–37.

Perman WH, Turski PA, Houston LW, Glover GH, Hayes CE. Methodology of in vivo human sodium MR imaging at 1.5 T. Radiology 1986; 160: 811–20.

Rovira A, Alonso J, Cucurella G, Nos C, Tintore M, Pedraza S, et al. Evolution of multiple sclerosis lesions on serial contrast-enhanced T1-weighted and magnetization-transfer MR images. AJNR Am J Neuroradiol 1999; 20: 1939–45.

Smith KJ, Kapoor R, Hall SM, Davies M. Electrically active axons degenerate when exposed to nitric oxide. Ann Neurol 2001; 49: 470–6.

Smith KJ, Lassmann H. The role of nitric oxide in multiple sclerosis. Lancet Neurol 2002; 1: 232–41.

Sontheimer H, Fernandez-Marques E, Ullrich N, Pappas CA, Waxman SG. Astrocyte Na+ channels are required for maintenance of Na+/K(+)-ATPase activity. J Neurosci 1994; 14: 2464–75.

Sontheimer H, Waxman SG. Ion channels in spinal cord astrocytes in vitro: II. Biophysical and pharmacological analysis of two Na+ current types. J Neurophysiol 1992; 68: 1001–11.

Thulborn KR, Davis D, Snyder J, Yonas H, Kassam A. Sodium MR imaging of acute and subacute stroke for assessment of tissue viability. Neuroimaging Clin N Am 2005; 15: 639–53, xi–xii.

Thulborn KR, Gindin TS, Davis D, Erb P. Comprehensive MR imaging protocol for stroke management: tissue sodium concentration as a measure of tissue viability in nonhuman primate studies and in clinical studies. Radiology 1999; 213: 156–66.

Turski PA, Perman WH, Hald JK, Houston LW, Strother CM, Sackett JF. Clinical and experimental vasogenic edema: in vivo sodium MR imaging. Work in progress. Radiology 1986; 160: 821–825.

van Waesberghe JH, Kamphorst W, De Groot CJ, van Walderveen MA, Castelijns JA, Ravid R, et al. Axonal loss in multiple sclerosis lesions: magnetic resonance imaging insights into substrates of disability. Ann Neurol 1999; 46: 747–54.

van Waesberghe JH, van Walderveen MA, Castelijns JA, Scheltens P, Lycklama a Nijeholt GJ, Polman CH, et al. Patterns of lesion development in multiple sclerosis: longitudinal observations with T1-weighted spin-echo and magnetization transfer MR. AJNR Am J Neuroradiol 1998; 19: 675–83.

van Walderveen MA, Kamphorst W, Scheltens P, van Waesberghe JH, Ravid R, Valk J, et al. Histopathologic correlate of hypointense lesions on T1-weighted spin-echo MRI in multiple sclerosis. Neurology 1998; 50: 1282–8.

Waxman SG. Conduction in myelinated, unmyelinated, and demyelinated fibers. Arch Neurol 1977; 34: 585–9.

Waxman SG. Axonal conduction and injury in multiple sclerosis: the role of sodium channels. Nat Rev Neurosci 2006; 7: 932–41.

Waxman SG, Black JA, Stys PK, Ransom BR. Ultrastructural concomitants of anoxic injury and early post-anoxic recovery in rat optic nerve. Brain Res 1992; 574: 105–19.